SALT PRECIPITATION DUE TO SC-GAS INJECTION: SINGLE VERSUS MULTI-POROSITY ROCKS

H. Ott[a,1], J. Snippe[1], K. de Kloe[1], H. Husain[2], and A. Abri[2]

(1) Shell Global Solutions International *BV*, The Netherlands.

(2) Study Center, Petroleum Development Oman, Muscat, Sultanate of Oman.

This paper was prepared for presentation at the International Symposium of the Society of Core Analysts held in Aberdeen, Scotland, UK, 27-30 August 2012

ABSTRACT

We investigate the consequences of formation dry-out due to the injection of under-saturated supercritical acid gas/CO_2 into a Middle Eastern dolomite formation for enhanced oil recovery (EOR) and acid gas (AG)/CO_2 disposal purposes. We perform core flood experiments and numerical simulations with the aim to highlight two aspects. Firstly, the risk assessment of injectivity loss associated with the precipitation of salt in the vicinity of an injection well for the respective EOR operation. Secondly, the rock matrix of the formation differs substantially from the simple sandstone of a previous study. The comparison of both rock types gives insight in the qualitatively different impact of salt precipitation on permeability/injectivity in a multi-porosity and a single porosity system, respectively.

INTRODUCTION

The injection of dry or under-saturated gases or supercritical (SC) fluids into water bearing formations might lead to a formation dry-out in the vicinity of the injection well [1-4]. The dry-out is caused by the evaporation/dissolution of formation water into the injected fluid and the subsequent transport of dissolved water in the injected fluid away from the injection well. Dry-out results in precipitation of solutes of the formation brine and consequently leads to a reduction of the rock's pore space and eventually to a reduction of permeability near the injection well, or even to the loss of injectivity [1]. This is considered as substantial risk for injection operations like the injection of acid gas and/or CO_2 into sedimentary rock formations for enhanced oil recovery (EOR) or sequestration. Mitigation methods such as fresh water injection to lower salt concentrations are considered, but are costly and not always possible or favorable for the respective injection operation. Consequently, an assessment of the risk of injectivity reduction is paramount for gas injection operations. The extent of the dry-out zone and the average porosity reduction can reliably be modeled by numerical simulations depending on the quality of available thermodynamic data, since it rather depends on the macroscopic mass balance than on the individual rock type and the microscopic processes [2]. The associated reduction of permeability, however, is rather of microscopic origin and depends on the exact location of the precipitate in the pore space and hence depends critically on the individual rock type and on the local flow regime. Experimental data is

scarce but crucial for a reliable evaluation, as several studies have shown that a modest reduction in porosity might lead to a substantial reduction in permeability [5-8] and, hence, to a serious impairment of injectivity.

The data presented in this paper is part of a study performed to assess the risk of injectivity loss due to salt precipitation in the formation around an injection well for EOR by miscible gas injection. The injection target is a Middle Easten dolomite reservoir with a multi-porosity rock matrix. The reservoir is at residual brine saturation (S_W~0.15) with the NaCl dominated brine being at the saturation limit (~ 280g/L). In the experiments we investigate the impact of salt precipitation by injecting dry SC-CO_2 into rock samples with different degrees of heterogeneity, at different water saturations, S_W, and with decane as proxy for the hydrocarbon phase. The experimental conditions are chosen to match key parameters for precipitation in the field as scaled from the field thermodynamic conditions and the field-fluids' properties. CO_2 was injected at residual water saturation to mimic the actual field scenario, and in 100% brine/water saturated samples as worst-case scenario and because of its relevance for CO_2 sequestration in saline aquifers. These experiments are directly comparable to an earlier study on a well-sorted sandstone (Berea) [9] and, hence, allow to study salt precipitation in multi-porosity versus single-porosity systems.

SALT PRECIPITATION IN WELL-SORTED SANDSTONE

In an earlier study we investigated salt precipitation in Berea sandstone [9]. By a combination of experiments and numerical simulations it was shown that there are different precipitation regimes depending on the CO_2 injection rate. Above a critical volumetric flow rate q_{cr}, the dry-out front propagates uniformly in the flow direction and salt precipitates in a uniform way, accordingly. Below q_{cr}, a negative water saturation gradient is possible, because substantially more water dissolves/evaporates close to the point of injection rather than further downstream, which might lead to a negative water-saturation gradient and consequently to a capillarity-driven backflow of brine in the direction of the injection point. The brine solutes are transported to the point of injection and precipitate there. As a consequence, it is possible to precipitate locally more salt than originally locally present dissolved in the brine phase, with the potential to block the pore space.

While below the critical flow rate, the capillary-driven backflow keeps the point of injection essentially brine-saturated, there is a downstream propagating dry-out region if the flow rate is above q_{cr}. If q_{cr} is reached, the dry-out front stops, since the water transport upstream, induced by capillary forces, matches the water transport downstream in the CO_2-rich phase. For this condition, salt precipitates at this local spot with a high change of pore space plugging. At this point the critical volumetric flow rate q_{cr} can be determined from the mass balance by:

$$q_{SC}\rho_{SC}X_{H2O,SC} = -q_{aq}\rho_{aq}X_{H2O,aq}, \quad (1)$$

where q_{SC} and q_{aq} are the volumetric fluxes of the CO_2-rich phase and the aqueous phase, ρ_{SC} and ρ_{aq} are the phase densities and $X_{H2O,SC}$ and $X_{H2O,aq}$ are the mass fractions of water in both phases, respectively.

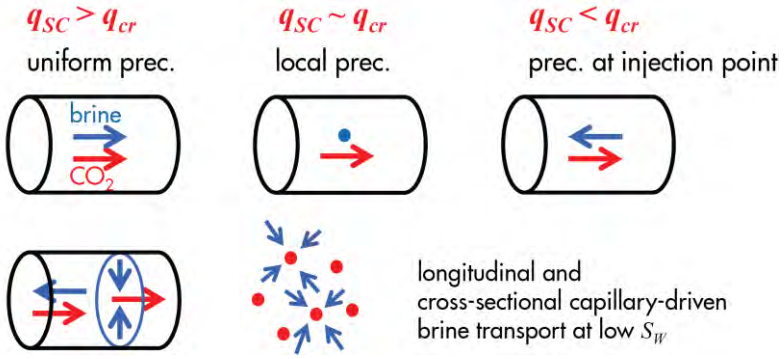

Figure 1: Top row: schematic view of the different flow regimes identified for simple pore systems (well-sorted sandstone). The flow regimes determine the precipitation pattern and are characterized by the flow rate with respect to a critical flow rate q_{cr}. Bottom row: schematic cross-sectional capillary-driven brine transport as described in the text.

The capillary-driven brine/salt transport explains qualitatively the experimentally observed solid-salt saturation in the longitudinal direction [9]. However, it does not explain the pressure data, and respectively the observed effective permeability during dry-out. In general, the effective permeability, $K_{eff,CO2}=K \cdot k_{r,CO2}$, might change due to the reduction of the absolute permeability K as consequence of salt precipitation, and due to relative permeability, $k_{r,CO2}$, because of the CO_2-saturation change during dry-out. Fig. 3 (further below) shows experimental pressure data during dry-CO_2 injection in Berea sandstone. The data are recorded under $q_{SC}>q_{cr}$ conditions showing a homogeneous precipitation profile. The pressure drop decreases over the experimental time according to an increasing effective permeability with a substantial mean solid-salt saturation of about 4.5% of the pore space. Even in the experiment reported in SCA2010-20 [9] with a local pore space occupation as high as 20%, the effective permeability improved during the experiment. The experimental results suggest salt precipitation in the vicinity of the CO_2-percolation pathways, leaving the cross-sectional area of these pathways essentially open.

As can be seen from this example, capillary rather than viscous-driven transport plays the key role at low S_W as typical for dry-out situations. The major difference, however, between single porosity sandstone and multi-porosity carbonate samples, as discussed in the following, can be expected in exactly these p_C-related properties.

MULTI-POROSITY DOLOMITE SAMPLES

The aim of the present study is to investigate the impact of salt precipitation due to the injection of dry AG/CO_2 into water containing rock for a Middle Eastern EOR project. The experiments were performed on reservoir rock samples. The rock matrix is dolomite-

based with 3 to 15wt% anhydrite and some halite. The sample porosities are between 0.05-0.22 and the permeability range between 1-300mD.

Exp	sample	K (mD)	ϕ	flooding sequence	salinity (wt% NaCl)	comments
B	Berea (10mm ∅)	500	0.22	brine - CO_2	20	P=100bar, T=45°C Fig.3, top panel
1	10	61	0.132	water - CO_2	0	Fig. 5
2	10	61	0.132	brine - CO_2	6	Fig. 5
3	3	97	0.184	water - CO_2	0	Fig. 3, top panel
4	3	97	0.184	brine - CO_2	6	Fig. 3, top panel
5	3	97	0.184	brine - decane - CO_2	12	
6	8	34	0.16	water - CO_2	0	
7	8	34	0.16	brine - CO_2	6	Fig. 3, bottom panel
8	8	34	0.16	brine - decane (cf) - CO_2	28	Fig. 3, bottom panel
9	14	307	0.178	brine - decane (cf) - CO_2	28	
10	7	33	0.142	brine - decane (cf) - CO_2	28	

Table 1: Samples and flooding sequences of the individual experiments. (cf) stands for centrifuge saturation resulting in a decane saturation at connate water.

The rock matrix shows a high degree of heterogeneity, both on a sample scale (one-inch diameter samples) and from sample to sample. Fig. 2 shows a typical example on the sample scale (photo and CT scan) and on the micro scale (SEM image): heterogeneous structures are observed on all scales resulting in a true multi-porosity system. MICP curves of all samples used in the present study are shown on the right-hand side of Fig. 2, reflecting the multi-porosity nature of the samples and the sample-to-sample variation. Berea data (red) is plotted for comparison.

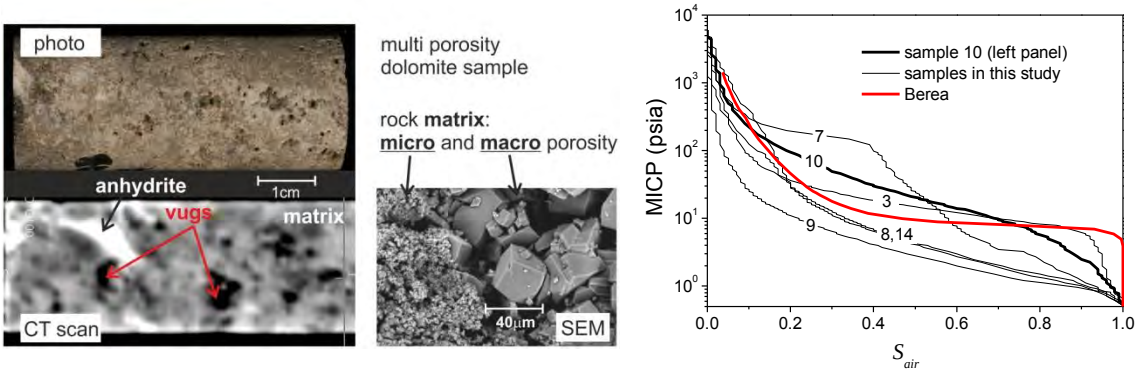

Figure 2: Left: Photo, CT scan and SEM image of a Middle Eastern rock sample (sample 10). Right: mercury-air capillary pressure (MICP) curves of different rock samples used in the present study. The images and MICP curves show the multi-porosity character of the rock matrix and the heterogeneity of the formation. Sample numbers are indicated in the plot (compare Table 1).

SC CO_2/AG is known to flow predominantly in regions of lowest entry pressure associated with highest permeability [10, 11]. Consequently, high-permeability samples (30-300mD) were selected for this study, with the porosity in the range between 0.13-0.19. Table 1 provides an overview of the studied samples and the flooding sequence as discussed further below.

CO_2-INJECTION EXPERIMENTS

The experiments were performed with a generic set of fluids: SC-CO_2 as acid-gas phase, decane as proxy for the hydrocarbon phase, and NaCl brines instead of the NaCl-dominated reservoir brine. The experimental conditions were P=110 bar and T=110°C and the CO_2 injection rate was 1.12 ml/min/cm^2, chosen to match the field conditions for the dry-out relevant parameters; based on previous experiments in sandstone, capillarity and the timescale of dry-out are key for the distribution of precipitates in the rock, and consequently for the permeability behaviour. Capillarity determines the solute transport at low S_W as discussed above and was matched in the present case by matching the capillary number, $N_{cap}=u\cdot\mu/\sigma$, with u and μ being the linear velocity of the injected fluid and its viscosity, and σ the respective CO_2/AG-brine interfacial tension. σ of the CO_2-brine system match over a wide P/T range the σ of the field case ($\sigma_{field}\approx\sigma_{exp}$), and hence, N_{cap} can be adjusted by $q_{exp}/q_{field}\approx\mu_{field}/\mu_{exp}$. The timescale of dry-out determines the crystallization process and is caused by the water transport in the injected fluid phase, which is determined by the solubility limit of water in the injected fluid phase ($\rho\cdot X$) and the injection rate q. We scale the rate by $q_{exp}\cdot\rho_{CO2}\cdot X_{H2O,CO2}\approx q_{field}\cdot\rho_{AG}\cdot X_{H2O,AG}$. Under experimental conditions, the water content in the CO_2 phase is $\rho_{CO2}\cdot X_{H2O,CO2}\sim 2\cdot 10^{-3}$ g/ml. The amount of precipitate depends on the immobile brine fraction that finally gets dissolved in the CO_2-rich phase. It was kept constant for all experiments by adjusting the brine salinity as further discussed in the text. In situ CT imaging shows no indication of salt accumulation due to macroscopic capillary-driven backflow as observed in the sandstone case for $q<q_{cr}$.

As worst-case scenario for the field case we performed experiments in 100% brine (water) pre-saturated samples, which also allows for direct comparison with the earlier experiments on sandstone. In subsequent experiments we introduced in two further steps the hydrocarbon phase as discussed in more detail below. The initial salinity has been chosen in all cases such that the same amount of salt precipitates in the sample, which requires an estimation of the immobile brine fraction by $k_r(S_W)$; this approach is valid, since viscous displacement (which does not lead to precipitation) and water evaporation (leading to solute enrichment and finally to salt precipitation) are acting predominantly on different time scales: minutes for viscous displacement versus hours for evaporation.

CO_2-injection experiments in 100% brine-saturated rock samples were performed on three different samples (Exp. 2, 4 and 7). As base case we performed experiments on the same samples in advance, but initially saturated with de-mineralized water to separate relative permeability effects from effects of precipitation on the effective permeability (Exp. 1, 3 and 6). Results are shown in the upper panel of Fig. 3 (Exp. 3 and 4). The base case (pure water experiment) shows, as expected, an increasing K_{eff} (decreasing ΔP) over time until the experiment was terminated after about 9 hours (after injection of ~ 150 PV). The experiment was repeated on the same rock sample and under the same conditions, but with the sample being brine-saturated instead of water. The brine salinity was 6wt% corresponding to about 1/4th of the field value assuming that about 50% of the

total water evaporates (on the high side). About 2.5 hours after the experiment was started, ΔP starts to deviate substantially from the base case which we interpret as the onset of precipitation since salinity reaches the saturation limit. ΔP increases steadily from then on until a maximum is reached after about 8 hours of CO_2 injection (130 PV injected), which we interpret as dry-out point. K_{eff} improves in the following, which is most likely due to the extraction of salt-bound water reducing the total volume of the precipitate. The permeability reduction observed in this experiment is more than two orders of magnitude (~350 compared to the base case). In all cases (Exp. 2, 4 and 7) we found permeability reductions of one to three orders of magnitude, probably depending on the exact pore structure (heterogeneity).

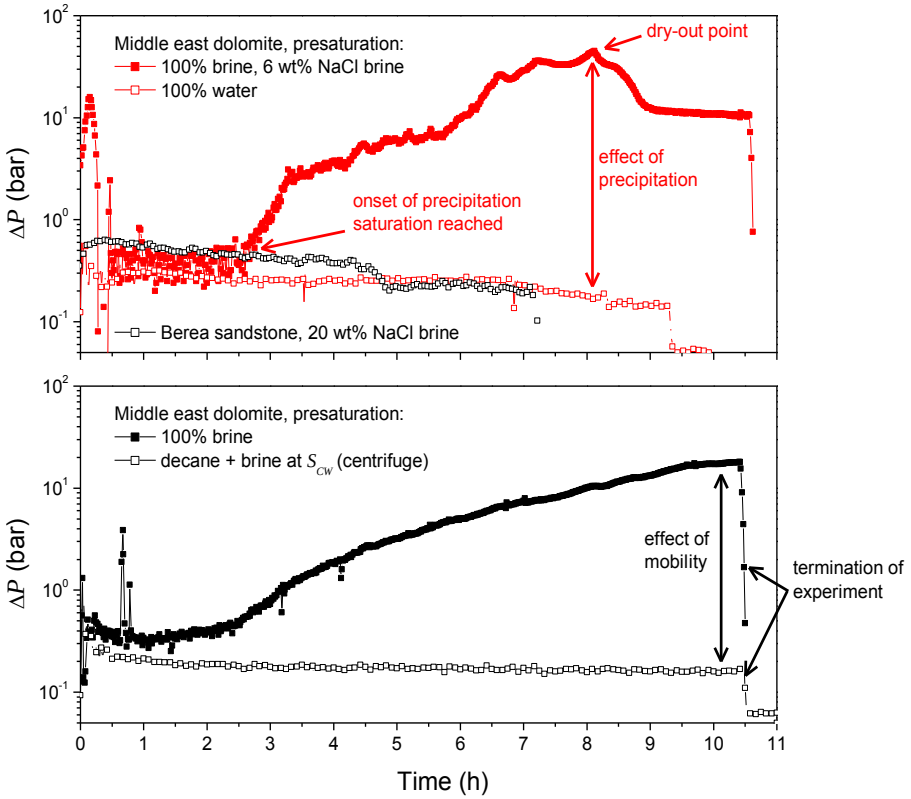

Figure 3: Pressure drop (ΔP) over the core during CO_2 injection. Upper panel: Experiment on Berea sandstone (black) and dolomite field samples (red), pre-saturated with an aqueous phase with water (open squares) and brine (filled squares). Lower panel: Experiments on a dolomite sample at 100% brine saturation (filled symbols) and pre-saturated with decane at residual water saturation.

In the next step we approximated to a system closer to the field case (Exp. 5). The sample was pre-saturated with brine (12wt% NaCl) and subsequently flooded with decane to displace brine without drying effect. After injection of 40 PV of decane, dry CO_2 was injected leading to a miscible displacement of the oil and to immiscible displacement of the brine phase and finally to evaporation of water. The difference compared to the aqueous experiment is that the brine phase has a reduced mobility after decane injection compared to the pure aqueous experiment. However, this experiment also showed a

reduction of permeability by more than two orders of magnitude (~250), comparable to the pure aqueous case. How comparable both experiments are is not clear, since we doubled the brine-salt concentration in anticipation of a much better brine displacement by decane than by CO_2, resulting in a lower water mobility.

In the final step we prepared the sample ex-situ by initial water/brine saturation and decane primary drainage in a centrifuge, to get the aqueous phase saturation down to true residual saturation as in the field case (Exp. 8-10). This results in an immobile water/brine phase in the sense of viscous displacement. The ex-situ prepared sample was then flooded with decane and was subsequently injected with CO_2 under otherwise the same conditions as in the previous experiments. The brine salinity was close to the saturation value (28wt% NaCl). The bottom panel of Fig. 3 shows the ΔP during the experiments (Exp. 7 and 8). Only a minor change of effective permeability was observed (in the order of equipment sensitivity), while the respective aqueous experiment (100% brine/water initial saturation) on the same sample showed a steady state after about 10 hours (220 PV injected), with a 110-fold reduction of permeability in line with the results observed previously. The result at residual brine saturation was reproduced in Exp. 9 and 10 on samples with different degrees of heterogeneity.

CONCEPTUAL MODEL

There is a clear qualitative difference between well-sorted sandstone and multi-porosity dolomite in the response to dry-out, and apparently, this difference is caused by the single-porosity versus multi-porosity nature of the rock types. In the following we develop a conceptual model, which captures the mechanism behind this, and which is already the first step in the direction of up-scaling and modeling dry-out in multi-porosity systems.

For CO_2-brine systems, CO_2 can be assumed to be the non-wetting phase entering the low p_C regions of the rock, generating preferred CO_2-flow pathways. We can further assume that these pathways are associated with the macro-porous subsystem. The micro porosity might serve as a brine reservoir and accordingly as a salt supply for the macro system, which is in contrast to the simple sandstone case without such a supply. Both subsystems will tend towards a capillary equilibrium at all time, and consequently the difference in capillary pressure resulting from the selective displacement is a transport mechanism of brine and of salt respectively, from the micro to the macro porous subsystem. This might lead to a higher salt accumulation in the macro porous system where the CO_2 is predominantly flowing and a reduction of K therein.

For simulating this conceptual model we use the Shell in-house reservoir simulator MoReS. With this model we do not aim to describe the experiments quantitatively in detail, but rather wish to explain the principal behavior and to attribute it to fundamental rock properties; despite the multi-porosity nature of the rock, for clarity and simplicity we consider a dual-porosity model. The model assumes the two subsystems as two separate

porous media in contact with each other. We expect to observe the effect already in a non-dimensional (0D) system, resulting in a simulation domain consisting of two grid blocks, one for each subsystem (with additional inlet and outlet pieces). Key parameters characterizing the properties of both subsystems are (1) the permeability and (2) the capillary pressure, $p_C(S_W)$. We assign a realistic permeability to the macro porous system, and make for simplicity the micro porous volume essentially impermeable in the direction of injection, which is a good approximation, since low-viscous CO_2 will flow in the pore space with the lowest entry pressure [11]. For lack of reliable CO_2-brine SCAL data, we estimate the magnitude of capillary pressure for both subsystems from the MICP data as shown in Fig. 2. The left panel of Fig. 4 shows $p_C(S_W)$ for both subsystems as used in the simulations; both saturation functions are the same, but for the micro system it is scaled by a factor of 8.

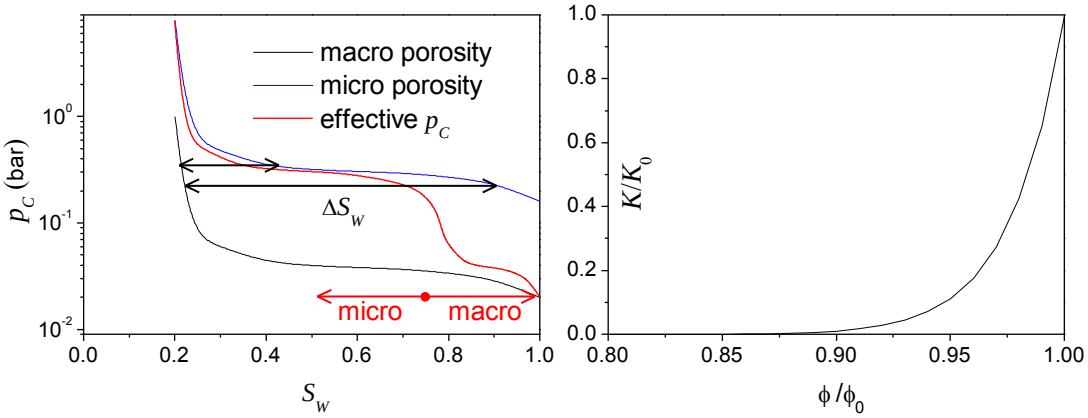

Figure 4: Left: capillary pressure curve $p_C(S_W)$ and the same curve scaled by a factor of 8. These curves are used for the simulations, representing $p_C(S_W)$ of the macro- and micro-porous subsystems, respectively. The red curve shows the approximate total p_C curve from the used p_C of micro and macro porosities and the volumetric ratio of both (25% macro porosity case). The arrows indicate a saturation difference between both subsystems in capillary equilibrium. Right: $K(\phi)$ relationship after Verma & Pruess and as used in the simulations (effectively applied to the macro porous subsystem).

The same relative permeability saturation functions $k_r(S_W)$ were assigned to both subsystems. $k_r(S_W)$ was determined from a fit to the experimental data from the dry-out of the water-saturated sample (shown in Fig. 5) where ΔP variation is determined by relative permeability only, excluding the effect of salt precipitation.

The reduction due to the precipitation-induced porosity change is modeled by introducing a $K(\phi)$ relationship as proposed by Verma and Pruess [6]:

$$\frac{K}{K_0} = \left(\frac{\Phi - \Phi_c}{1 - \Phi_c} \right)^n , \qquad (2)$$

with K_0 being the initial absolute permeability, Φ being the actual porosity normalized to the initial porosity ϕ_0, ϕ/ϕ_0, and Φ_c, being the normalized critical porosity at which the permeability vanishes. The function can be tuned by the exponent n and Φ_c. We used a sharp function with a loss of permeability at a solid-salt saturation of about 10% of the pore volume as shown in the right-hand panel of Fig. 4.

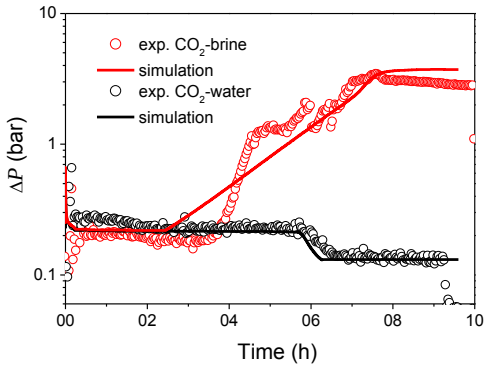

Figure 5: Pressure difference Δ*P* measured during dry-out of a brine- (Exp. 2: red symbols) and water- (Exp. 1: black symbols) saturated carbonate rock sample, and the respective simulations as described in the text.

Fig. 5 shows the result of a simulation in comparison to one of the experiments. Note that we do not aim for a quantitative model, but for the mechanism and an order of magnitude match. The experimental Δ*P* has been matched by variation of the volumetric ratio of the macro porosity volume to the total simulation domain as explained further below. Both sets of experimental data are well described by the same model, assuming a dry-out of a pure water phase for the base case and a brine phase with the salinity of the actual experiment. In this case we find an absolute permeability reduction by a factor of ~20. It is important to note that the step-like function of the base case (pure-water) with the long-lasting plateau and rapid decline cannot be described assuming a simple porosity structure.

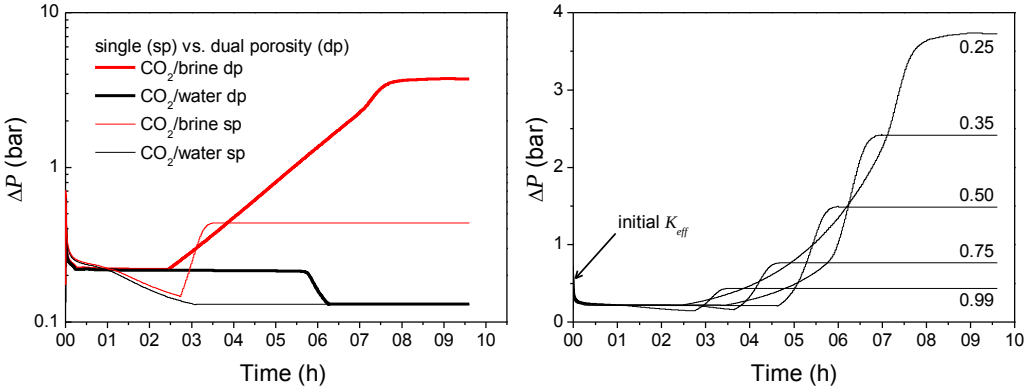

Figure 6: Δ*P* during dry-out of a single-porosity and dual-porosity system (left). The simulation domain was initially saturated with water (black lines) for the base case without salt precipitation, and with brine (red lines). Right: Δ*P* of the brine pre-saturated system for different volumes of macro porosity V_{mac}/V_{total}.

In the following we would like to highlight some of the relevant properties of the model. The simulated Δ*P* is most sensitive to (1) the *K*(ϕ) relationship with which the effect of salt precipitation on injectivity is introduced, and (2) the ratio of the macro-porosity to the total porosity. Of fundamental interest are the borderline cases of single-porosity and dual-porosity systems.

The left-hand panel of Fig. 6 shows simulations of CO_2 floods in porous media with 25% macro porosity (dual-porosity system) and 99% macro porosity (single-porosity system), using otherwise the same model and parameters (in particular the total porosity).
We simulated the base case with pure water, showing only the effect of relative permeability, and the actual dry-out of a brine phase under the otherwise same simulation settings. The single porosity case mainly differs from the dual or multi-porosity case with respect to the dry-out time, and - more importantly - in the degree of permeability reduction. The single porosity case shows a shorter time until a steady state (or full dry-out) is reached. This is due to the water/brine storage property of the micro porosity leading to a more gradual release of water to the CO_2 phase in case of dual porosity. As the right-hand panel of Fig. 6 shows, a gradual change of the volume fraction of the macro porous system, V_{mac}/V_{total}, gradually changes both properties, the permeability reduction and the delay time.

In contrast to the dual-porosity case, which shows a clear impairment of injectivity, in the single-porosity case the effective permeability improved from the initial to the final state of the CO_2 flood. But the model shows a dip in the ΔP curve caused by the relative permeability effect setting in faster than precipitation occurs. The Berea experimental data does not show such a dip, but a steadily decreasing ΔP as shown in Fig. 3. This difference between the Berea experiment and the simulation can be explained by the salt concentration of the brine, which was close to the saturation limit in the Berea experiment, in contrast to the dilute brine used in the present simulation and in the carbonate experiments. As a consequence, in the simulation more time is needed to reach the salt saturation limit, and hence precipitation occurs at a time where k_r has already increased $K_{eff,CO2}$.

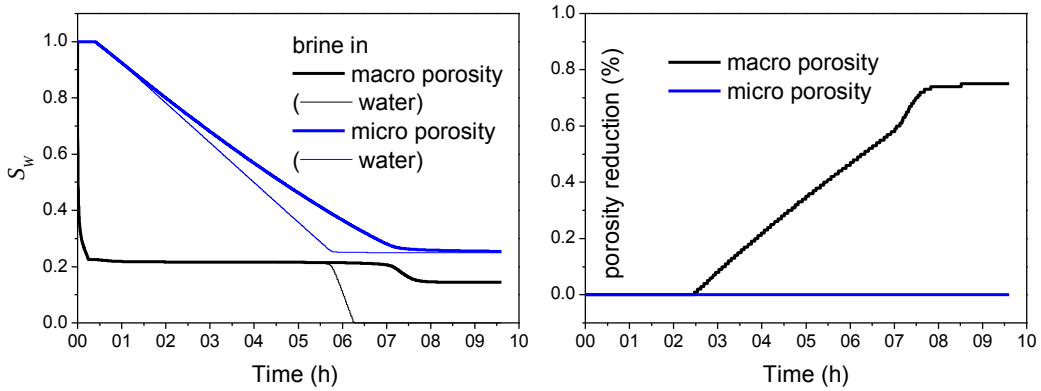

Figure 7: Simulation results of the dual-porosity system. Left: water- (thin lines) and brine- (thick lines) saturation (respectively 1-S_{CO2}) in the macro (black) and micro (blue) porous subsystem.[b] Right: porosity reduction in the macro (black) and micro (blue) porous subsystem due to salt precipitation. The volume corresponds to the density of dry salt.

Fig. 7 shows the simulated water/brine saturation, S_W (left), and the porosity reduction due to salt precipitation (right) for both the single-porosity and dual-porosity case. A

rapid de-saturation to a value close to residual brine/water saturation is observed in the macro porous system, while the de-saturation in the micro-porosity follows a rather linear trend, caused by the constant CO_2-injection rate and the associated constant water transport by evaporation and transport into and in the CO_2 phase in the macro-porous system. Since the CO_2 phase flows only in the macro porous system, the behaviour of S_W reflects the brine transport from the micro to the macro porous system. The same simulation with pure water leads to a qualitatively similar picture, but with a shorter dry-out time due to the solubility limit of water in the CO_2-phase for different salinities and with a full dry out of the macro system after about 6 hours. An interesting behaviour shows the porosity as a function of time. The salt, coming mainly from the micro-porous system, is precipitated only in the macro-porous system with no precipitation in the micro porosity.

SUMMARY AND CONCLUSIONS

We investigated the impact of salt precipitation on injectivity during acid-gas/CO_2 injection in a dolomite-based reservoir rock by means of core flood experiments. The impairment of the injectivity has been found to depend on the mobility of the brine phase, with a potentially high impairment at high water saturations; salt precipitation in the investigated field samples led to a strong decrease of permeability in cases where the brine phase was above residual saturation, i.e. with a mobile brine phase. Which means that above residual water saturation there is a potential risk of injectivity loss. At residual saturation, as in the present field case, i.e. with an immobile brine phase, the effective permeability is not affected; from these experiments we expect no risk of injectivity loss for the current EOR project, however, there is a strong risk for a sequestration project in saline aquifers in similar formations.

The observed behaviour in the pure aqueous case in the multi-porosity dolomite is in strong contrast to the behaviour that has been observed in sandstone, where the effective permeability improved during injection (relative permeability effect vs. effect of precipitation). Apparently this is caused by the multi-porosity nature of the dolomite rock matrix compared to the simple well-sorted sandstone. The underlying mechanism has been identified by numerical simulations of single and dual-porosity systems, and the experimental observations have been qualitatively (semi-quantitatively) reproduced. In the dual-porosity model, micro-porous volume acts as a brine reservoir gradually supplying brine and salt respectively to the CO_2-conducting macro-porous system. Solid salt has been found to precipitate only in the porosity class conducting the CO_2. With a given $K(\phi)$ relationship the volumetric ratio of macro to micro-porosity determines the degree of permeability reduction, explaining the improving effective permeability in simple sandstone and the strong reduction in the dolomite-based multi-porosity reservoir rock. This effect is amplified by the effectively reduced CO_2-conductive cross-section due to the presence of the micro-porous subsystem.

ACKNOWLEDGEMENTS

The authors thank Steffen Berg for useful discussions and for reviewing the manuscript. Fons Marcelis and Ton Blok are acknowledged for sample characterization and MICP measurements.

REFERENCES

a. Corresponding author; e-mail address: holger.ott@shell.com, research@holger-ott.de

b. The water remaining in the micro porosity after dry-out (~0.25) corresponds to the residual water saturation of $k_r(S_W)$. The water saturation in the macro porosity corresponds to 1-S_{CO2}, and includes the solid salt saturation.

1. K. Pruess and J. García, Multiphase Flow Dynamics During CO_2 Injection into Saline Aquifers, *Environmental Geology,* Vol. 42, pp. 282-295, 2002.
2. R. C. Fuller, J. H. Prevost and M. Piri, Three-Phase Equilibrium and Partitioning Calculations for CO_2 Sequestration in Saline Aquifers, *J. Geophys. Res.,* Vol., 111, 2006.
3. T. Giorgis, M. Carpita and A. Battistelli, 2D Modeling of Salt Precipitation During the Injection of Dry CO_2 in a Depleted Gas Reservoir, *Energy Conv. Managemt.,* Vol. 48, pp. 1816–1826, 2007.
4. S. Hurter, D. Labregere and J. Berge, Simulations for CO_2 Injection Projects with Compositional Simulator, *SPE-108540*, presented at Offshore Europe 2007 conference of the Society of Petroleum Engineers, Aberdeen, Scotland, September 2007.
5. P. J. Vaughan, D. E. Moore, C. A. Morrow and J. D. Byerlee, Role of Cracks in Progressive Permeability Reduction During Flow of Heated Aqueous Fluid Through Granite, *J. Geophys. Res.*, Vol. 91, No. B7, pp. 7517–7530, 1986.
6. A. Verma and K. Pruess, Thermohydrologic Conditions and Silica Redistribution Near High-Level Nuclear Wastes Emplaced in Saturated Geological Formations, *Journal of Geophysical Res.*, Vol. 93 (B2), pp. 1159-1173, 1988.
7. H. Pape, C. Clauser and J. Iffland, Permeability Prediction Based on Fractal Pore-Space Geometry, *Geophysics,* Vol. 64, No. 5, pp. 1447-1460, 1999.
8. T. Xu, Y. Ontoy, P. Molling, N. Spycher, M. Parini and K. Pruess, Reactive Transport Modeling of Injection Well Scaling and Acidizing at Tiwi Field, Philippines, *Geothermics,* Vol. 33, No. 4, pp. 477-491, 2004.
9. H. Ott, K. de Kloe, C. Taberner, F. Marcelis, Y. Wang, A. Makurat, Rock/Fluid Interaction by Injection of Supercritical CO_2/H_2S: Investigation of Dry-zone Formation Near the Injection Well, International Symposium of the Society of Core Analysts, Halifax, Nova Scotia, Canada, October 4-7, 2010, **SCA2010-20**.
10. H. Ott, S. Berg, S. Oedai: Displacement and Mass Transfer in CO_2/Brine in Sandstone, International Symposium of the Society of Core Analysts, Austin, Texas, USA, September 18-21, 2011, **SCA2011-05**.
11. S. Berg, S. Oedai, and H. Ott: Displacement and Mass Transfer Between Saturated and Unsaturated CO_2–Brine Systems in Sandstone, International Journal of Greenhouse Gas Control, Article in Press, available online (2011).